Journal of Materials Chemistry A

ROYAL SOCIETY OF CHEMISTRY

COMMUNICATION

View Article Online
View Journal | View Issue

Cite this: J. Mater. Chem. A, 2020, 8, 20925

Received 6th August 2020
Accepted 28th September 2020

DOI: 10.1039/d0ta07705d

rsc.li/materials-a

Graphdiyne-based Pd single-atom catalyst for semihydrogenation of alkynes to alkenes with high selectivity and conversion under mild conditions†

Xue-Peng Yin,[a] Shang-Feng Tang,[a] Chao Zhang,[a] Hong-Juan Wang,*[a] Rui Si,*[b] Xiu-Li Lu*[a] and Tong-Bu Lu*[a]

The development of efficient heterogeneous catalysts for alkyne hydrogenation with high activity and selectivity is highly desirable and yet remains a great challenge. Herein, a Pd single-atom catalyst (Pd^{s}–GDY) is prepared using graphdiyne as support, and used in the semihydrogenation of alkynes. As a proof of concept, the Pd^{s}–GDY exhibits a high activity for the semihydrogenation of phenylacetylene under mild reaction conditions, with a TOF of 6290 h^{-1}, and a selectivity of 99.3% at 100% conversion, both much higher than those of the counterparts comprising Pd nanoparticles (NPs), namely, Pd^{NP1}–GDY (with 2 nm Pd NPs) and Pd^{NP2}–GDY (with 12 nm Pd NPs). In addition, after the full conversion of phenylacetylene, Pd^{s}–GDY could still maintain a selectivity as high as 98.9% towards styrene, with almost no phenylethane produced even with a prolonged reaction time; in contrast, for Pd^{NP1}–GDY and Pd^{NP2}–GDY, within the same reaction time, the selectivity decreases dramatically to 66.6% and 8.5%, respectively. Infrared spectroscopy reveals that Pd^{s}–GDY features the weakest adsorption to styrene, which is responsible for its high performance. This work provides an effective strategy to rationally design Pd catalysts for semihydrogenation of alkynes to alkenes with desirable activity and selectivity.

Introduction

Semihydrogenation of alkynes to alkenes is of great importance on account of the extensive applications of alkenes in chemical industry, such as agrochemicals, vitamins, polymers, and olefin metathesis.[1–5] Up to now, palladium(Pd)-based catalysts are most used in this area because of their outstanding hydrogenation activities; however, they typically suffer from low selectivities due to further hydrogenation of alkenes (a phenomenon also known as over-hydrogenation).[6–9] In order to restrain the over-hydrogenation, many methods have been developed;[10–16] for example, Pd metal could be modified by lead or quinoline (*e.g.*, Lindlar catalyst) to suppress the hydrogenation of alkenes and thus to improve the selectivity in semihydrogenation of alkynes. However, these Pd-based catalysts are often toxic and not environment-friendly. Another efficient strategy to achieve desirable selectivity is fabricating bimetallic catalysts through alloying Pd with metals such as In, Ag, Pb, and Cu, also known as the "site-isolating" structural modification.[17–20] For example, Feng *et al.* reported that PdIn(110) surface with atomic Pd sites has a high catalytic selectivity for semihydrogenation of acetylene, with 92% selectivity for ethylene at 90 °C, much higher than that of $Pd_3In(111)$ surface with Pd trimer sites.[17] However, the "site-isolating" structural modification of Pd-based catalysts could not enable the high exposure of active sites (which only reside on the surface of alloys), thus leading to low utilization of Pd atoms and a poor atom economy. In either case above, Pd-based heterogeneous catalysts can hardly achieve high activity simultaneously with outstanding selectivity under mild reaction conditions. Therefore, it is highly desirable to develop Pd-based catalysts with high TOF, high conversion, excellent selectivity, and good stability for semihydrogenation of alkynes.

Recently, as a new emerging class of heterogeneous catalysts, single-atom catalysts (SACs) featuring isolated metal atoms anchored on solid supports have shown great advantages in water splitting, oxygen reduction, CO_2 reduction, and organic synthesis, by virtue of their maximized atomic utilization as well as unique structures.[21–29] In particular, for noble-metal-based catalysts, the utmost atomic utilization can dramatically decrease the material cost. In addition, benefiting from the relatively uniform structure of metal atoms with low coordination numbers therein, many SACs show high selectivities and activities in the catalytic process.[30] It has been shown that Pd SACs fabricated on various supports give higher activities for

[a]MOE International Joint Research Laboratory of Materials Microstructure, Institute for New Energy Materials and Low Carbon Technologies, School of Materials Science and Engineering, Tianjin University of Technology, Tianjin 300384, People's Republic of China. E-mail: hongjuanwang@tjut.edu.cn; luxiuli@email.tjut.edu.cn; lutongbu@tjut.edu.cn

[b]Shanghai Synchrotron Radiation Facility, Shanghai Institute of Applied Physics, Chinese Academy of Sciences, Shanghai 201204, China. E-mail: sirui@sinap.ac.cn

† Electronic supplementary information (ESI) available. See DOI: 10.1039/d0ta07705d

hydrogenation of alkynes to alkenes, compared with Pd nanoparticle counterparts.[31–35] However, a high conversion and a high selectivity could not be simultaneously achieved for these Pd SACs, unless (in a few cases) under an extremely high H_2 pressure. For example, isolated Pd species anchored on TiO_2 support (Pd–TiO_2) show a high selectivity (>90%) and high conversion (99%) for semihydrogenation of phenylacetylene to styrene at a high H_2 pressure of 1.0 MPa, and yet the conversion decreases dramatically to 16% at 0.4 MPa H_2 pressure owing to the limited catalytic activity of Pd SACs.[35] Thus, it remains a challenge to achieve both high selectivity and high activity for semihydrogenation of alkyne under mild conditions.

As a new carbon material, graphdiyne (GDY) features the unique butadiyne linkages between benzene rings, which could serve as the sites to stabilize isolated metal atoms of low valence, and thus enable high catalytic activities.[36–38] Herein, on the basis of the unique structure of GDY, we prepared three types of Pd–GDY catalysts, comprising Pd single atoms (denoted as Pd^S–GDY) and two types of Pd nanoparticles with sizes around 2 nm (Pd^{NP1}–GDY) and 12 nm (Pd^{NP2}–GDY). The catalytic performances of these Pd–GDY catalysts in semihydrogenation of alkynes show an evident dependence on the size of Pd species under room temperature and 0.2 MPa H_2 pressure. Remarkably, Pd^S–GDY displays an outstanding catalytic activity, with TOF up to 6290 h^{-1} at 100% conversion with 99.3% selectivity in hydrogenation of phenylacetylene to styrene. Moreover, Pd^S–GDY shows almost no activity for the further hydrogenation of styrene, even when the reaction is kept going on after the full conversion of phenylacetylene. By contrast, for Pd^{NP1}–GDY and Pd^{NP2}–GDY, they both display the unwanted abilities to further hydrogenate styrene, and show much lower activities for styrene production. And their selectivities for styrene drop to 66.6% and 8.5% after 3 h hydrogenation. The experimental results indicated that the higher catalytic performance of Pd^S–GDY originates from the weaker adsorption of styrene on Pd single atoms compared with the cases on Pd nanoparticles in Pd^{NP1}–GDY and Pd^{NP2}–GDY. In addition, Pd^S–GDY also shows high performances for the semihydrogenation of some other alkynes, including 1-octyne, 3-octyne, and diphenylacetylene.

Results and discussion

In this study, the Pd–GDY catalysts were prepared by simple wet-chemistry routes as shown in Scheme 1. First, GDY powder was synthesized from hexaethynylbenzene by a modified Hay–Glaser coupling reaction. The sp-hybridized alkynyl carbon atoms in GDY provide the sites for anchoring Pd atoms. Through controlling the reaction solvent and temperature, Pd^S–GDY, Pd^{NP1}–GDY, and Pd^{NP2}–GDY were obtained. Specifically, for the preparation of Pd^S–GDY, GDY powder (10 mg) was dispersed in DMF (5 mL) to obtain a dispersion of GDY. Then K_2PdCl_4 (470 μL, 10 mM) was added into the above dispersion, and the mixture was stirred for 2 h at 0 °C to obtain Pd^S–GDY. In contrast, Pd^{NP1}–GDY and Pd^{NP2}–GDY were prepared by replacing the DMF with deionized water and regulating the reaction temperatures (0 °C for Pd^{NP1}–GDY and 60 °C for Pd^{NP2}–GDY).

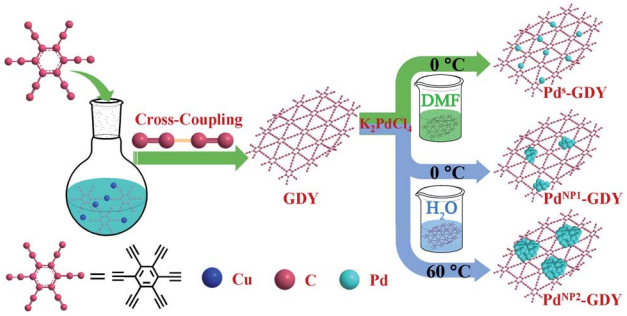

Scheme 1 Illustration for the preparation of Pd^S–GDY, Pd^{NP1}–GDY, and Pd^{NP2}–GDY.

The prepared GDY was characterized by Raman and X-ray photoelectron spectroscopy (XPS). As shown in Fig. S1a,† the Raman spectrum shows four distinct peaks at 1420 cm^{-1} (D band), 1578 cm^{-1} (G band), 1924 cm^{-1}, and 2163 cm^{-1}, respectively, in which the peaks at 1924 cm^{-1} and 2163 cm^{-1} can be attributed to the vibration of conjugated diyne linkers, in good accordance with those reported in the literatures.[39,40] In addition, the high-resolution XPS of C 1s of GDY in Fig. S1b† could be deconvoluted into four subpeaks, in which the peak at 285.1 eV was assigned to the C≡C (sp).[40] And the atomic ratio of sp/sp^2 is approximately 2, which is consistent with the chemical composition of GDY. The microstructure and composition of Pd–GDY catalysts were further investigated by transmission electron microscopy (TEM), high-resolution transmission electron microscopy (HR-TEM), and high-angle annular dark-field scanning transmission electron microscopy (HAADF-STEM). As shown in Fig. 1a, no Pd clusters or nanoparticles were observed in the TEM image of Pd^S–GDY; in contrast, the average

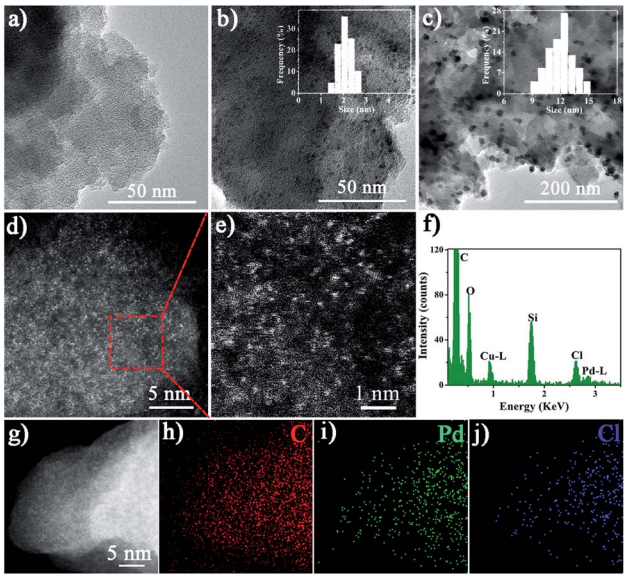

Fig. 1 (a–c) TEM images of Pd^S–GDY (a), Pd^{NP1}–GDY (b), and Pd^{NP2}–GDY (c). (d and e) HAADF-STEM image (d) and the enlarged HAADF-STEM image (e) of (d) of Pd^S–GDY. (f) EDS spectrum for Pd^S–GDY. (g–j) EDS mapping images of Pd^S–GDY.

sizes of Pd nanoparticles in Pd^{NP1}–GDY and Pd^{NP2}–GDY were about 2 and 12 nm, respectively (Fig. 1b and c). As shown in Fig. 1d and e of Pd^{S}–GDY, abundant isolated Pd atoms can be observed in GDY because of the different *Z* contrast of Pd and C. The energy dispersive spectroscopy (EDS) (Fig. 1f) shows that the C, Pd, and Cl elements coexist in the sample of Pd^{S}–GDY (the other elements come from the Cu grid). Moreover, the elemental mapping images for Pd^{S}–GDY reveal the uniform spatial distributions of C, Pd, and Cl over the entire structure (Fig. 1g–j). Furthermore, the X-ray diffractometer (XRD) pattern in Fig. S2† confirms that no crystalline Pd species is formed in Pd^{S}–GDY. For Pd^{NP1}–GDY and Pd^{NP2}–GDY, the XRD patterns (Fig. S2†) display peaks at $2\theta = 40.1°$, which could be assigned to the (111) plane of metallic Pd, indicating the formation of Pd nanoparticles. In addition, the HR-TEM images in Fig. S3 and S5† show clear fringes of 0.22 nm, which can be ascribed to the (111) lattice plane of cubic-phase Pd, in good accordance with the XRD results. Moreover, the HR-TEM images and corresponding elemental mapping images of Pd^{NP1}–GDY and Pd^{NP2}–GDY confirm the distribution of Pd nanoparticles on the support of GDY (Fig. S4 and S6†). The surface area, pore volume, and pore size distribution of Pd^{S}–GDY, Pd^{NP1}–GDY, and Pd^{NP2}–GDY were analyzed by measuring the N_2 adsorption–desorption isotherms at 77 K (Fig. S7†), the specific surface area of Pd^{S}–GDY, Pd^{NP1}–GDY, and Pd^{NP2}–GDY were 25.0, 21.5, and 21.0 $m^2 g^{-1}$, respectively. In addition, the average pore sizes and pore volume for Pd^{NP1}–GDY are almost the same as those of Pd^{S}–GDY (Table S1†). However, the average pore sizes and pore volume of Pd^{NP2}–GDY have obvious decrease compared with those of Pd^{S}–GDY and Pd^{NP1}–GDY. This phenomenon could be attributed to much larger size of Pd nanoparticles (12 nm) in Pd^{NP2}–GDY than those in Pd^{NP1}–GDY(2 nm) and Pd^{S}–GDY (atomic Pd sites), bringing to the coverage of some mesopores in GDY supports.

Further insights into the electronic and structural information on these Pd–GDY catalysts were obtained from XPS and X-ray absorption fine structure (XAFS) spectroscopy. As demonstrated in Fig. 2a, for Pd 3d, the two main peaks located at 338.3 and 343.6 eV could be attributed to Pd $3d_{5/2}$ and Pd $3d_{3/2}$ in K_2PdCl_4. These two peaks in Pd^{S}–GDY shift to lower binding energy at 337.7 and 342.8 eV, which are higher than that of Pd^0 (336.0 and 341.3 eV) and lower than that of Pd^{2+} (338.3 and 343.6 eV), demonstrating that Pd atoms are positively charged $Pd^{\delta+}$ ($0 < \delta < 2$), indicating the strong interaction between Pd atoms and GDY. For Pd^{NP1}–GDY and Pd^{NP2}–GDY, the two peaks could be divided into four peaks at 336.0, 337.7, 341.3, and 342.8 eV, which could be ascribed to the coexistence of Pd^0 and $Pd^{\delta+}$, further confirming the formation of Pd nanoparticles.[41] In addition, as shown in Fig. S8,† the Raman peaks attributed to the vibration of conjugated diyne links in Pd^{S}–GDY, Pd^{NP1}–GDY, and Pd^{NP2}–GDY were not as prominent as those for GDY, indicating the interaction between Pd species and –C≡C–C≡C– moieties.[36] Furthermore, more detailed structural information for Pd^{S}–GDY was obtained from the Pd K-edge X-ray absorption near-edge structure (XANES) spectra and extended X-ray absorption fine structure (EXAFS) spectra. As shown in Fig. 2b, the near-edge feature of Pd^{S}–GDY is between those of Pd foil and PdO, confirming the slightly positively charged Pd species, in good consistency with the XPS results. Moreover, as shown by the FT-EXAFS spectra in Fig. 2c, the Pd foil displays a distinct peak at about 2.8 Å, which is attributed to the Pd–Pd bond. In the FT-EXAFS of Pd^{S}–GDY, only the peak centered at the distance of *ca.* 2.0 Å was observed and no Pd–Pd contribution was found, further confirming that Pd atoms are atomically dispersed on the surface of GDY. In order to unveil the coordination environment around Pd in Pd^{S}–GDY, its FT-EXAFS curve was fitted in *R* space. The fitting results shown in Table S2† demonstrate that on average each Pd atom coordinates with two C and two Cl atoms.

Semihydrogenation of alkynes to alkenes is of great importance in the chemical industry.[41] As a proof of concept, the catalytic performances of Pd^{S}–GDY, Pd^{NP1}–GDY, and Pd^{NP2}–GDY in phenylacetylene hydrogenation was tested in an autoclave in ethanol solvent under 0.2 MPa pressure hydrogen at 25 °C. As shown in Fig. 3a, the Pd–GDY catalysts exhibit distinct size-dependent performances on the hydrogenation of phenylacetylene. The conversion of phenylacetylene and the selectivity for styrene and phenylethane as a function of reaction time over the prepared catalysts are shown in Fig. 3b–d. As shown in Fig. 3b, the highest selectivity toward styrene for Pd^{NP2}–GDY is only 59.7% with 86.4% conversion, and the selectivity is reduced to 8.5% at 100% conversion of phenylacetylene after reaction for 3 h. For Pd^{NP1}–GDY, as shown in Fig. 3c, it achieves 95.8% selectivity with 100% conversion after reaction for 2 h; however, Pd^{NP1}–GDY subsequently catalyzes the hydrogenation of styrene to phenylethane and displays only 66.6% selectivity to styrene after 3 h reaction. By stark contrast, for Pd^{S}–GDY, the selectivity toward styrene could reach at 99.3% with 100% conversion of phenylacetylene at 2 h (Fig. 3d), and even with prolonged reaction time, the further hydrogenation of styrene is effectively suppressed, which is beneficial for the styrene separation. In brief, the hydrogenation properties on Pd^{NP2}–GDY, Pd^{NP1}–GDY, and Pd^{S}–GDY are quite different (Fig. 3a and e) and show a prominent size-dependence. After the 100% conversion of phenylacetylene, Pd^{S}–GDY shows the best catalytic performance, including a highest TOF of 6290 h^{-1} for styrene production with 99.3% selectivity; in contrast, the TOF values

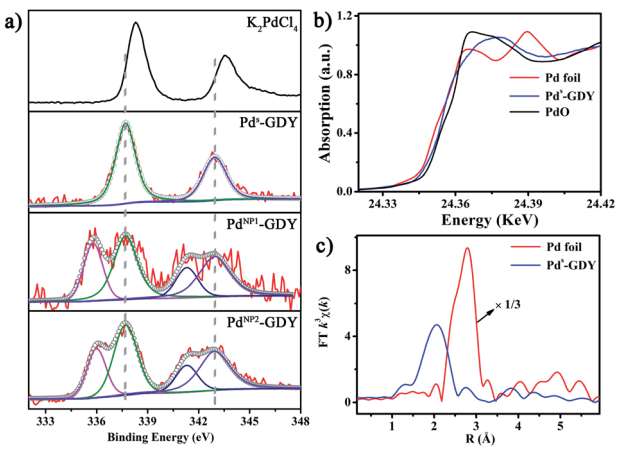

Fig. 2 (a) Core-level Pd 3d XPS of Pd^{S}–GDY, Pd^{NP1}–GDY, Pd^{NP2}–GDY, and K_2PdCl_4. (b and c) Pd K-edge XANES (b) and FT-EXAFS spectra (c) of Pd^{S}–GDY, with Pd foil and PdO as reference.

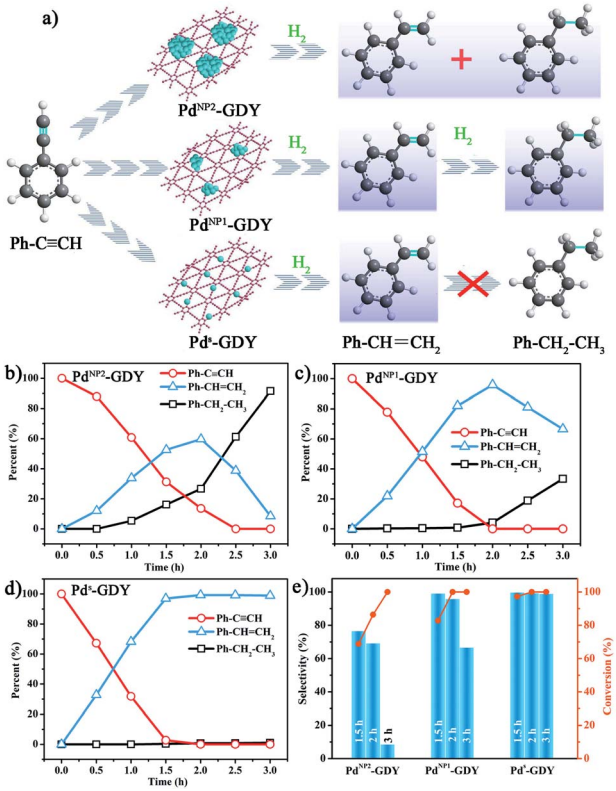

Fig. 3 (a) Illustration showing different hydrogenation processes of phenylacetylene over different Pd–GDY catalysts. (b–d) The conversion of phenylacetylene and the selectivity toward styrene and phenylethane as a function of reaction time over Pd^{NP2}–GDY (b), Pd^{NP1}–GDY (c), and Pd^{S}–GDY (d). (e) The comparison of catalytic performances for Pd^{S}–GDY, Pd^{NP1}–GDY, and Pd^{NP2}–GDY catalysts. Reaction conditions: 2 mg catalyst, 1.0 mmol phenylacetylene, 2 mL ethanol, 25 °C, 0.2 MPa H_2.

(and selectivity) were 4551 h^{-1} (95.8%) for Pd^{NP1}–GDY and 1270 h^{-1} (38.8%) for Pd^{NP2}–GDY (Table S4†). Durability and recyclability of catalysts are critical for practical applications. To test the durability of Pd^{S}–GDY, the catalyst after a test run was collected and washed for subsequent recycling.[42] As shown in Fig. S9,† the selectivity and activity were still high with negligible changes after five recycling tests. In addition, we have measured the semihydrogenation performance of Pd^{S}–GDY at 50 °C. As shown in Fig. S10,† the reaction rate for the hydrogenation of phenylacetylene at 50 °C was greatly improved compared with that at 25 °C. In addition, Pd^{S}–GDY still shows high selectivity (>99%) to styrene at 100% conversion of phenylacetylene. In addition, the TEM image, Pd 3d XPS spectra, HAADF-STEM images and Raman spectra after the catalytic test were shown in Fig. S11–S14,† indicating that Pd^{S}–GDY has a high stability in semihydrogenation of phenylacetylene. Besides, As shown in Fig. S15† the Cl 2p XPS spectra of Pd^{S}–GDY was analyzed showing the corresponding binding energies at 198.5 eV (Cl–Pd) and 200.3 eV (Cl–C).[43] In addition, the amounts of chlorine showed no obvious decrease after the catalytic test, further indicating the stability of Pd^{S}–GDY (Table S5†).

To further investigate the performance of Pd^{S}–GDY in semihydrogenation of alkynes to alkenes, a series of additional experiments were conducted. As shown in Table S6,† GDY gives no activity for hydrogenation of phenylacetylene, demonstrating that the active sites derived from the Pd species in Pd^{S}–GDY, Pd^{NP1}–GDY, and Pd^{NP2}–GDY. As a comparison, hydrogenations of phenylacetylene were also performed on Pd/C–D (Pd nanoparticles prepared on mesoporous carbon in DMF solution) and commercial Pd/C under the same conditions (Fig. S17 and Table S6†). It is shown that Pd/C–D and Pd/C converts phenylacetylene completely to phenylethane after reacting for 2 h, demonstrating no selectivity toward styrene. Notably, even in a reactant with a molar ratio of 1/9 (phenylacetylene/styrene), Pd^{S}–GDY still displays a high activity for the semihydrogenation of phenylacetylene to styrene with 100% conversion and 99.9% selectivity, and only trace phenylethane was detected. Moreover, as shown in Fig. S18,† when the reaction system was scaled up by elevating the amount of phenylacetylene, Pd^{S}–GDY maintains a high catalytic performance. Furthermore, Pd^{S}–GDY could also be used as the catalyst for semihydrogenation of other alkynes (such as 1-octyne, 3-octyne, and diphenylacetylene) with high performances (Table S6†). These results further confirm the unique advantages of Pd^{S}–GDY in selective hydrogenation.

The strong size-dependent activity of the Pd–GDY catalysts for the hydrogenation of alkynes may originate from the different adsorption ability for alkenes.[44] To understand the adsorption properties of Pd^{S}–GDY, we recorded the FT-IR spectra of all Pd–GDY catalysts after exposure to styrene and subsequent removal of free styrene. As shown in Fig. S19,† the peaks of vibrational signals attributed to –C≡C– shift to lower wavenumber because of the interaction with Pd species in the Pd–GDY catalysts, and the intensities of the vibrational signals increase in the order of Pd^{S}–GDY < Pd^{NP1}–GDY < Pd^{NP2}–GDY, indicating the weakest binding capability of Pd single atoms in Pd^{S}–GDY to styrene molecules. As a result, Pd^{S}–GDY shows the best performance for semihydrogenation of phenylacetylene to styrene and demonstrates almost no ability for the further hydrogenation of styrene to phenylethane.

Conclusions

In conclusion, we developed facile strategies to prepare Pd–GDY catalysts, including Pd^{S}–GDY, Pd^{NP1}–GDY, and Pd^{NP2}–GDY. The HAADF-STEM and XAFS analyses of the Pd^{S}–GDY confirmed the isolated Pd atoms anchored on GDY support. The Pd^{NP1}–GDY and Pd^{NP2}–GDY samples contain Pd nanoparticles with size about 2 and 12 nm, respectively. The prepared Pd–GDY catalysts exhibit strong size-dependent activities for the hydrogenation of alkynes. Benefiting from the weak adsorption ability to styrene, Pd^{S}–GDY shows a superior activity and selectivity in semihydrogenation of phenylacetylene to styrene, compared with Pd^{NP1}–GDY, Pd^{NP2}–GDY and commercial Pd/C catalyst. This work not only designs a highly efficient Pd single-atom catalyst for selective hydrogenation reaction under mild reaction conditions but also provides the understanding of the correlation between the size of Pd species and hydrogenation performance.

Experimental section

Materials

Potassium chloropalladite (K_2PdCl_4), phenylacetylene (536-74-3), 1-octyne (629-05-0), 3-octyne (15232-76-5) and diphenylacetylene (501-65-5) purchased from energy-chemical (Shanghai, China). Ethanol and DMF purchased from Sinopharm Chemical Reagent Co., Ltd (Shanghai, China). All reagents were of analytical grade and used without further purification. The GDY powder was synthesized according to Li's work.[45] Ultra-pure water with a resistivity of 18.2 MΩ was used in all synthesis.

Catalyst preparation

Pd^S–GDY. In a typical synthesis of Pd^S–GDY, 10 mg GDY powder was uniformly dispersed in 5 mL DMF solution to obtain a dispersion of GDY. Then 470 μL 10 mM K_2PdCl_4 was put into the above dispersion and stirred for 2 h at 0 °C. The resulting product was washed several times with DMF and ethanol and dried under vacuum at 50 °C.

Pd^{NP1}–GDY and Pd^{NP2}–GDY. The preparation methods of Pd^{NP1}–GDY and Pd^{NP2}–GDY were similar to those of Pd^S–GDY. 10 mg GDY was uniformly dispersed in 5 mL H_2O to obtain a dispersion of GDY. Then 470 μL 10 mM K_2PdCl_4 was put into the above dispersion and stirred for 2 h at 0 °C and 60 °C, respectively. The Pd^{NP1}–GDY and Pd^{NP2}–GDY were finally obtained after washing several times with H_2O and ethanol and dried under vacuum at 50 °C.

Pd/C–D. In detail, 10 mg mesoporous carbon powder was uniformly dispersed in 5 mL DMF solution to obtain a dispersion of mesoporous carbon. Then 470 μL K_2PdCl_4 (10 mM) and 200 mL $NaBH_4$ (4 mg mL^{-1}) was put into the above dispersion and stirred for 2 h at 0 °C. The resulting product was washed several times with DMF and ethanol and dried under vacuum at 50 °C.

Catalyst testing

Liquid-phase hydrogenation of phenylacetylene (536-74-3), 1-octyne (629-05-0), 3-octyne (15232-76-5), and diphenylacetylene (501-65-5) were performed in a 50 mL stainless steel autoclave. 2.0 mg of catalyst was placed into the autoclave with 2.0 mL of ethanol (as a solvent) and 1.0 mmol alkyne under magnetic stirring at 25 °C. After the system was purged with hydrogen gas for three times, 0.2 MPa of H_2 pressure remained. When the reaction time was reached, products were tested by Thermo Trace1300 gas chromatography equipped with a flame ionization detector. The signals of alkyne, alkene, and alkane (as the reactant, desirable product, and byproduct respectively in semihydrogenation of alkyne) were recorded. Catalytic activity and selectivity were calculated as follows:

$$\text{Conversion } (\%) = \frac{\text{moles of converted reactants}}{\text{moles of reactants in feed}} \times 100$$

$$\text{Selectivity } (\%) = \frac{\text{moles of desirable products}}{\text{moles of converted reactants}} \times 100$$

Characterization

X-ray diffraction (XRD) patterns were obtained on SmartLab 9KW equipped with Cu Kα radiation (λ = 1.5147 Å). Transmission electron microscopy (TEM) characterization was recorded using a Tecnai G2 Spirit TWIN at an acceleration voltage of 120 KV. Aberration-corrected scanning transmission electron microscope (STEM) images were performed using a Titan Cubed Themis G2 300 equipped with a Probe Corrector. X-ray photoelectron spectra (XPS) data were collected on an ESCALAB250Xi with the Al Kα radiation as the X-ray source. All binding energies were calibrated based on the C 1s peak at 284.8 eV. Raman spectra were obtained on high resolution laser confocal fiber Raman spectrometer (HORIBA EVOLVTION, HORIBA Jobinyvon, France) at the excitation wavelength of 532 nm. The actual Pd loadings were analyzed by the inductively coupled plasma-mass spectrometry (ICP-MS, iCAP RQ). The X-ray absorption fine structure (XAFS) spectra at Pd K-edge (E_0 = 24350 eV) was performed at BL14W1 beamline of Shanghai Synchrotron Radiation Facility (SSRF) operated at 3.5 GeV under "top-up" mode with a constant current of 250 mA. The XAFS data were recorded under fluorescence mode with a Lytle-type ion chamber. The energy was calibrated accordingly to the absorption edge of pure Pd foil. Athena and Artemis codes were used to extract the data and fit the profiles. For the X-ray absorption near edge structure (XANES) part, the experimental absorption coefficients as function of energies $\mu(E)$ were processed by background subtraction and normalization procedures, and reported as "normalized absorption" with E_0 = 24350 eV for all the tested samples and Pd foil/PdO standard. For the extended X-ray absorption fine structure (EXAFS) part, the Fourier transformed (FT) data in R space were analyzed by applying first-shell approximate model for Pd–C and Pd–Cl contributions. The passive electron factors, S_0^2, were determined by fitting the experimental data on Pd foils and fixing the coordination number (CN) of Pd–Pd to be 12, and then fixed for further analysis of the measured samples. The parameters describing the electronic properties (*e.g.*, correction to the photoelectron energy origin, E_0) and local structure environment including CN, bond distance (R) and Debye–Waller factor around the absorbing atoms (σ^2) were allowed to vary during the fit process. The fitted ranges for k and R spaces were selected to be k = 3–11 $Å^{-1}$ or 3–12 $Å^{-1}$ with R = 1–3 Å (k^2 weighted).

Conflicts of interest

There are no conflicts to declare.

Acknowledgements

This work was supported by the National Key R&D Program of China (2017YFA0700104), the National Natural Science Foundation of China (21790052 and 21805207), 111 Project of China (D17003) and the Science & Technology Development Fund of Tianjin Education Commission for Higher Education (2018KJ129).

Notes and references

1 K. Choe, F. Zheng, H. Wang, Y. Yuan, W. Zhao, G. Xue, X. Qiu, M. Ri, X. Shi, Y. Wang, G. Li and Z. Tang, *Angew. Chem., Int. Ed.*, 2020, **59**, 3650–3657.

2 F. Studt, F. Abild-Pedersen, T. Bligaard, R. Z. Sorensen, C. H. Christensen and J. K. Norskov, *Science*, 2008, **320**, 1320–1322.

3 Y. Liu, X. Liu, Q. Feng, D. He, L. Zhang, C. Lian, R. Shen, G. Zhao, Y. Ji, D. Wang, G. Zhou and Y. Li, *Adv. Mater.*, 2016, **28**, 4747–4754.

4 H. Liang, B. Zhang, H. Ge, X. Gu, S. Zhang and Y. Qin, *ACS Catal.*, 2017, **7**, 6567–6572.

5 Y. Cao, H. Zhang, S. Ji, Z. Sui, Z. Jiang, D. Wang, F. Zaera, X. Zhou, X. Duan and Y. Li, *Angew. Chem., Int. Ed.*, 2020, **59**, 11647–11652.

6 L. Kuai, Z. Chen, S. Liu, E. Kan, N. Yu, Y. Ren, C. Fang, X. Li, Y. Li and B. Geng, *Nat. Commun.*, 2020, **11**, 48.

7 X. Zhao, L. Zhou, W. Zhang, C. Hu, L. Dai, L. Ren, B. Wu, G. Fu and N. Zheng, *Chem*, 2018, **4**, 1080–1091.

8 M. Crespo-Quesada, F. Cárdenas-Lizana, A.-L. Dessimoz and L. Kiwi-Minsker, *ACS Catal.*, 2012, **2**, 1773–1786.

9 T. Mitsudome, T. Urayama, K. Yamazaki, Y. Maehara, J. Yamasaki, K. Gohara, Z. Maeno, T. Mizugaki, K. Jitsukawa and K. Kaneda, *ACS Catal.*, 2015, **6**, 666–670.

10 Z. Wang, L. Yang, R. Zhang, L. Li, Z. Cheng and Z. Zhou, *Catal. Today*, 2016, **264**, 37–43.

11 D. Mei, M. Neurock and C. M. Smith, *J. Catal.*, 2009, **268**, 181–195.

12 B. Yang, R. Burch, C. Hardacre, G. Headdock and P. Hu, *J. Catal.*, 2013, **305**, 264–276.

13 G. Vilé, D. Albani, N. Almora-Barrios, N. López and J. Pérez-Ramírez, *ChemCatChem*, 2016, **8**, 21–33.

14 M. Armbruster, K. Kovnir, M. Behrens, D. Teschner, Y. Grin and R. Schlogl, *J. Am. Chem. Soc.*, 2010, **132**, 14745–14747.

15 G. Kyriakou, M. B. Boucher, A. D. Jewell, E. A. Lewis, T. J. Lawton, A. E. Baber, H. L. Tierney, M. Flytzani-Stephanopoulos and E. C. Sykes, *Science*, 2012, **335**, 1209–1212.

16 D. Albani, M. Shahrokhi, Z. Chen, S. Mitchell, R. Hauert, N. Lopez and J. Perez-Ramirez, *Nat. Commun.*, 2018, **9**, 2634.

17 Q. Feng, S. Zhao, Y. Wang, J. Dong, W. Chen, D. He, D. Wang, J. Yang, Y. Zhu, H. Zhu, L. Gu, Z. Li, Y. Liu, R. Yu, J. Li and Y. Li, *J. Am. Chem. Soc.*, 2017, **139**, 7294–7301.

18 G. X. Pei, X. Y. Liu, A. Wang, A. F. Lee, M. A. Isaacs, L. Li, X. Pan, X. Yang, X. Wang, Z. Tai, K. Wilson and T. Zhang, *ACS Catal.*, 2015, **5**, 3717–3725.

19 W. Niu, Y. Gao, W. Zhang, N. Yan and X. Lu, *Angew. Chem., Int. Ed.*, 2015, **54**, 8271–8274.

20 G. X. Pei, X. Y. Liu, X. Yang, L. Zhang, A. Wang, L. Li, H. Wang, X. Wang and T. Zhang, *ACS Catal.*, 2017, **7**, 1491–1500.

21 X. Li, W. Bi, L. Zhang, S. Tao, W. Chu, Q. Zhang, Y. Luo, C. Wu and Y. Xie, *Adv. Mater.*, 2016, **28**, 2427–2431.

22 H. Fei, J. Dong, Y. Feng, C. S. Allen, C. Wan, B. Volosskiy, M. Li, Z. Zhao, Y. Wang, H. Sun, P. An, W. Chen, Z. Guo, C. Lee, D. Chen, I. Shakir, M. Liu, T. Hu, Y. Li, A. I. Kirkland, X. Duan and Y. Huang, *Nat. Catal.*, 2018, **1**, 63–72.

23 Y. Zheng, Y. Jiao, Y. Zhu, Q. Cai, A. Vasileff, L. H. Li, Y. Han, Y. Chen and S. Z. Qiao, *J. Am. Chem. Soc.*, 2017, **139**, 3336–3339.

24 N. Zhang, T. Zhou, M. Chen, H. Feng, R. Yuan, C. a. Zhong, W. Yan, Y. Tian, X. Wu, W. Chu, C. Wu and Y. Xie, *Energy Environ. Sci.*, 2020, **13**, 111–118.

25 Y. Qu, Z. Li, W. Chen, Y. Lin, T. Yuan, Z. Yang, C. Zhao, J. Wang, C. Zhao, X. Wang, F. Zhou, Z. Zhuang, Y. Wu and Y. Li, *Nat. Catal.*, 2018, **1**, 781–786.

26 X. Rong, H. J. Wang, X. L. Lu, R. Si and T. B. Lu, *Angew. Chem., Int. Ed.*, 2020, **59**, 1961–1965.

27 X. Wang, Z. Chen, X. Zhao, T. Yao, W. Chen, R. You, C. Zhao, G. Wu, J. Wang, W. Huang, J. Yang, X. Hong, S. Wei, Y. Wu and Y. Li, *Angew. Chem., Int. Ed.*, 2018, **57**, 1944–1948.

28 X. L. Lu, X. Rong, C. Zhang and T. B. Lu, *J. Mater. Chem. A*, 2020, **8**, 10695–10708.

29 H. Zhou, Y. Zhao, J. Gan, J. Xu, Y. Wang, H. Lv, S. Fang, Z. Wang, Z. Deng, X. Wang, P. Liu, W. Guo, B. Mao, H. Wang, T. Yao, X. Hong, S. Wei, X. Duan, J. Luo and Y. Wu, *J. Am. Chem. Soc.*, 2020, **142**, 12643–12650.

30 A. Wang, J. Li and T. Zhang, *Nat. Rev. Chem.*, 2018, **2**, 65–81.

31 Q. Feng, S. Zhao, Q. Xu, W. Chen, S. Tian, Y. Wang, W. Yan, J. Luo, D. Wang and Y. Li, *Adv. Mater.*, 2019, **31**, e1901024.

32 S. Zhou, L. Shang, Y. Zhao, R. Shi, G. I. N. Waterhouse, Y. C. Huang, L. Zheng and T. Zhang, *Adv. Mater.*, 2019, **31**, e1900509.

33 F. Huang, Y. Deng, Y. Chen, X. Cai, M. Peng, Z. Jia, P. Ren, D. Xiao, X. Wen, N. Wang, H. Liu and D. Ma, *J. Am. Chem. Soc.*, 2018, **140**, 13142–13146.

34 G. Vile, D. Albani, M. Nachtegaal, Z. Chen, D. Dontsova, M. Antonietti, N. Lopez and J. Perez-Ramirez, *Angew. Chem., Int. Ed.*, 2015, **54**, 11265–11269.

35 F. Yang, S. Ding, H. Song and N. Yan, *Sci. China Mater.*, 2020, **63**, 982–992.

36 X. P. Yin, H. J. Wang, S. F. Tang, X. L. Lu, M. Shu, R. Si and T. B. Lu, *Angew. Chem., Int. Ed.*, 2018, **57**, 9382–9386.

37 L. Hui, Y. Xue, H. Yu, Y. Liu, Y. Fang, C. Xing, B. Huang and Y. Li, *J. Am. Chem. Soc.*, 2019, **141**, 10677–10683.

38 Y. Xue, B. Huang, Y. Yi, Y. Guo, Z. Zuo, Y. Li, Z. Jia, H. Liu and Y. Li, *Nat. Commun.*, 2018, **9**, 1460.

39 Y. Y. Han, X. L. Lu, S. F. Tang, X. P. Yin, Z. W. Wei and T. B. Lu, *Adv. Energy Mater.*, 2018, **8**, 1702992.

40 Y. Fang, Y. Xue, Y. Li, H. Yu, L. Hui, Y. Liu, C. Xing, C. Zhang, D. Zhang, Z. Wang, X. Chen, Y. Gao, B. Huang and Y. Li, *Angew. Chem., Int. Ed.*, 2020, **59**, 13021–13027.

41 N. Yang, H. Cheng, X. Liu, Q. Yun, Y. Chen, B. Li, B. Chen, Z. Zhang, X. Chen, Q. Lu, J. Huang, Y. Huang, Y. Zong, Y. Yang, L. Gu and H. Zhang, *Adv. Mater.*, 2018, **30**, e1803234.

42 G. Ji, Y. Duan, S. Zhang, B. Fei, X. Chen and Y. Yang, *ChemSusChem*, 2017, **10**, 3427–3434.

43 Y. Zhao, W. Liang, Y. Li and L. Lefferts, *Catal. Today*, 2017, **297**, 308–315.

44 R. Guo, Q. Chen, X. Li, Y. Liu, C. Wang, W. Bi, C. Zhao, y. Guo and M. Jin, *J. Mater. Chem. A*, 2019, **7**, 4714–4720.

45 G. Li, Y. Li, H. Liu, Y. Guo, Y. Li and D. Zhu, *Chem. Commun.*, 2010, **46**, 3256–3258.

